Evolution of the electronic structure of HoB_4 with temperature

Deepnarayan Biswas,[1] Nishaina Sahadev,[1] Ganesh Adhikary,[1] Geetha Balakrishnan,[2] and Kalobaran Maiti[1,*]

[1]*Department of Condensed Matter Physics and Materials' Science, Tata Institute of Fundamental Research, Colaba, Mumbai 400 005, India*

[2]*Department of Physics, University of Warwick, Coventry CV4 7AL, United Kingdom*

(Received 17 June 2013; revised manuscript received 7 August 2013; published 7 October 2013)

We studied the electronic structure of a Shastry-Sutherland lattice system, HoB_4 employing high-resolution photoemission spectroscopy and *ab initio* band-structure calculations. The surface and bulk borons exhibit subtle differences and loss of boron compared to the stoichiometric bulk. However, the surface and bulk conduction bands near Fermi level are found to be similar. Evolution of the electronic structure with temperature is found to be similar to that observed in a typical charge-disordered system. A sharp dip is observed at the Fermi level in the low-temperature spectra revealing a signature of antiferromagnetic gap. Asymmetric spectral weight transfer with temperature manifests particle-hole asymmetry that may be related to the exotic properties of these systems.

DOI: 10.1103/PhysRevB.88.134405 PACS number(s): 75.50.Ee, 71.23.−k, 79.60.Ht, 74.62.En

I. INTRODUCTION

Physics of disorder is one of the most challenging issues in material science as it is hard to avoid disorder in real systems arising from defects, imperfections, etc. While it is hard to probe these natural effects, some lattice structures possess intrinsic disorder on the basis of electronic interactions leading to exotic properties providing pathways to probe disorder induced effects on the electronic properties. Shastry-Sutherland lattice is one such realization, where the strong diagonal exchange interaction J_2 forms spin dimers. Competition between J_2 and interdimer interactions J_1 leads to an interesting phase diagram involving a spin-liquid phase, a long-range ordered phase, etc.[1] A plethora of exotic phases could be derived via tuning some control parameters; e.g., J. Liu *et al.* showed that charge-carrier doping (electron or hole) in such systems leads to strong asymmetry in the electronic properties—while hole doping renormalizes spin-spin interactions leading to superconductivity, electron doped systems can be metallic but nonsuperconducting.[2] Varieties of fields have emerged based on these spin-disordered parent systems. Experimental realization of these effects are not so common due to the paucity of materials exhibiting such structures. Most of the studies so far are centered around the compound $SrCu_2(BO_3)_2$, where Cu^{2+} has a spin-half state and forms the Shastry-Sutherland lattice exhibiting interesting phenomena.[3]

Recently, it was observed that rare-earth tetraborides possess structure and magnetic interactions akin to the Shastry-Sutherland lattice as shown in Fig. 1. The diagonal magnetic interaction J_2 between the rare-earth moments shown in the figure are strong forming spin dimers. These materials exhibit diversified electronic and magnetic properties depending on interaction J_1 among these dimers relative to J_2.[4,5] For example, CeB_4 and YbB_4 do not exhibit long-range order, while PrB_4 orders ferromagnetically at low temperatures and most of the other tetraborides order antiferromagnetically.[6,7] Some of them exhibit multiple magnetic phase transitions at low temperature.[8] For example, TbB_4 exhibits noncollinear magnetic structure with two antiferromagnetic phase transitions.[9] Noncollinear magnetism with quadrupole strain and multiple phase transition is observed in DyB_4.[5]

HoB_4 is one among the complex tetraborides exhibiting multiple magnetic transitions and noncollinear magnetism.[10] The crystal structure of HoB_4 is tetragonal[8] with $a = 7.085$ Å and $c = 4.004$ Å. Depending upon the symmetry of the boron sites, there are three nonequivalent borons: B1 (apical) and B3 (equatorial) form octahedra, and B2 forms boron dimers connecting the boron octahedra. The interaction among Ho moments are mediated by the borons. The spin-spin interactions in the ab plane as shown in Fig. 1(b) correspond to a Shastry-Sutherland-type lattice. HoB_4 exhibits two antiferromagnetic transitions: at $T_{N1} = 7.1$ K, it exhibits an incommensurate antiferromagnetic ordering. The magnetic structure becomes commensurate at $T_{N2} = 5.7$ K.[11] Resistivity and transport measurements in the presence of magnetic field exhibit an anomalous phase diagram involving varieties of metamagnetic phase.[12] Evidently, HoB_4 is complex exhibiting a plethora of interesting phases and one of the ideal systems to study disorder induced effects in the electronic structure. Here, we studied the electronic structure of HoB_4 employing high-resolution photoemission spectroscopy and *ab initio* band-structure calculations. Interesting surface-bulk features are observed in the experimental spectra. The evolution of the electronic structure appears to be similar to that observed for charge-disordered systems.

II. EXPERIMENT

Single crystalline sample of HoB_4 was grown using mirror furnace[13] and characterized by x-ray diffraction, Laue pattern, transport, and magnetic measurements revealing high quality of the sample. Photoemission measurements were carried out using a R4000 WAL electron analyzer from Gammadata Scienta and monochromatic photon sources, Al $K\alpha$ (1486.6 eV), He I (21.2 eV), and He II (40.8 eV) radiations. The resolution of the instrument was set to 450, 5, and 10 meV for Al $K\alpha$, He I, and He II measurements respectively. An open cycle He cryostat was used to get the temperature variation from room temperature to 10 K. The base pressure of the chamber was better than 5×10^{-11} torr during measurements. The sample was extremely hard with no cleavage plane. We fractured the sample by using a top post to expose clean surface. We also verified the sample surface by scraping using a small grain diamond file. The angle integrated spectral features obtained from both types of surface preparations were

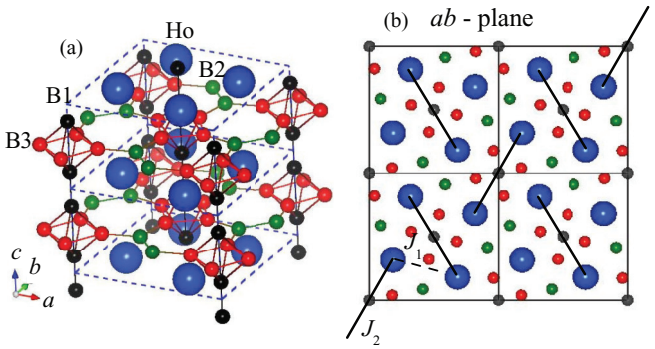

FIG. 1. (Color online) (a) Crystal structure of HoB_4. (b) ab plane containing Ho and B atoms. The lines show strong antiferromagnetic coupling between Ho sites that form spin dimers as proposed in a Shastry-Sutherland lattice.

identical. Reproducibility of the spectra was ensured after each trial of surface cleaning procedures.

The energy-band structure was calculated using the full potential linearized augmented plane-wave method within the local-density approximation (LDA) using WIEN2K software.[14] The energy convergence was achieved using 1000 k points within the first Brillouin zone. The tetragonal crystal structure[8] of HoB_4 was considered for the calculations. Convergence was achieved for the paramagnetic ground state considering both energy and charge convergence criteria. In order to introduce electron-electron Coulomb repulsion among Ho $4f$ electrons, U, into the calculation, we have employed the LDA + U method considering an effective electron interaction strength U_{eff} (= $U - J$; J = Hund's exchange integral was set to zero following Anisimov *et al.*[15]) for various values of U_{eff} up to about 7 eV.

III. RESULTS AND DISCUSSIONS

The probing depth of the photoemission spectroscopic technique can be varied by changing the electron emission angle. Following this procedure, we studied the core-level spectra using Al $K\alpha$ photon energy, where the mean escape depth λ for valence electrons is close to ~20 Å.[16] λ can be made half of its normal emission value if the photoelectron emission angle is made 60° with respect to the surface normal. The Ho $4d$ core-level spectra shown in Fig. 2(a) exhibit an identical line shape for normal emission and 60° angled emission geometries indicating similar surface and bulk electronic structures for the electronic states associated to Ho. B $1s$ spectra, however, exhibit modifications with the change in λ. There is an overall decrease in the intensity of the B $1s$ peak by about 10% in the 60° angled spectrum indicating a loss of boron on the surface compared to bulk. The B $1s$ spectra exhibit two distinct features around 187- and 187.7-eV binding energies—the relative intensity of these features changes with the change in surface sensitivity, suggesting the surface borons to be somewhat different from the bulk borons.

The valence-band spectra shown in Fig. 2(c) are identical at both the emission geometries. The near Fermi level ϵ_F part is rescaled and shown in Fig. 2(c) exhibiting an unaltered line shape with the change in surface sensitivity. This is curious as the intensities near ϵ_F are largely constituted by B $2p$

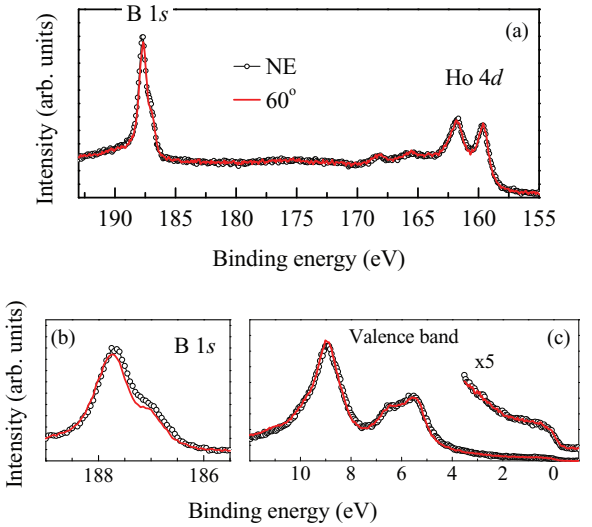

FIG. 2. (Color online) (a) B $1s$ and Ho $4d$ core-level spectra obtained at normal emission and 60° angle with surface normal. The expanded part of B $1s$ spectra are shown in (b). (c) Valence-band spectra and its rescaled part near ϵ_F for normal and 60° angled emission.

states and surface borons exhibit subtle differences. These results suggest that the influence of disorder on the conduction electrons dominates over the translational symmetry breaking occurring at the surface.

Photoemission being a quantum-mechanical process, the spectral features represent the eigenstates of the excited-state Hamiltonian. If the electron correlation is finite in a system, these final states, which have a hole due to photoemission, differ significantly from the initial eigenstates and multiple features appear in the photoemission spectra associated to a different level of screening of the photoholes, multiplet splitting, etc. The well screened feature is usually termed as the main peak and other features are called satellites. Conduction electrons consisting of the hybridized states of Ho ($5d6s$) states and B $2p$ states are expected to be weakly correlated as both possess a large degree of itineracy due to large orbital extensions. It is notable here that the electron correlation among Ho $4f$ electronic states is strong. However, these states primarily appear far away from ϵ_F making Ho ($5d6s$) states and B $2p$ contributions dominant at ϵ_F. Thus, satellites are not expected in this system. In contrast, the core-level spectra of Ho exhibit significant final-state effects with distinct satellite features. This is found in all the core-level spectra as depicted in Figs. 3(a) and 3(b) for the $4d$ and $5p$ spectra, respectively. Presence of the satellites indicates that electron-electron interaction cannot be neglected in this system as also observed in various other $4d$ and $5d$ systems.[17] A change in temperature down to 10 K does not influence the spectral line shape.

B $1s$ spectra, on the other hand, are significantly influenced by the temperature—a gradual shift towards lower binding energy is observed in Fig. 3(c) with the decrease in temperature, which cannot be represented by a rigid shift of the experimental spectrum. Three distinct features, A, B, and C are required to simulate the experimental spectra at any temperature as shown in Fig. 3(e). The linewidth (~0.74 eV), energy separation (~0.7 eV), and relative intensity of the features

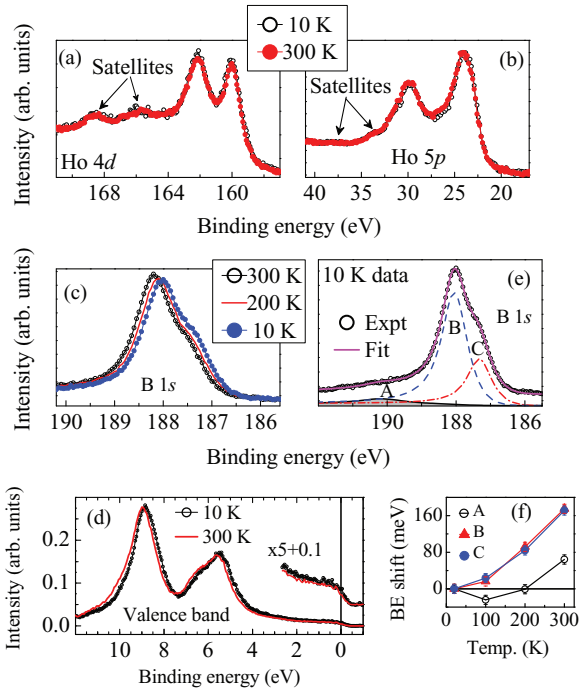

FIG. 3. (Color online) Temperature evolution of (a) Ho 4*d*, (b) 5*p*, (c) B 1*s*, and (d) valence-band spectra. (e) Fit to the B 1*s* spectrum; lines are the fit curves. (f) Energy shift of the component peaks with respect to 10-K data.

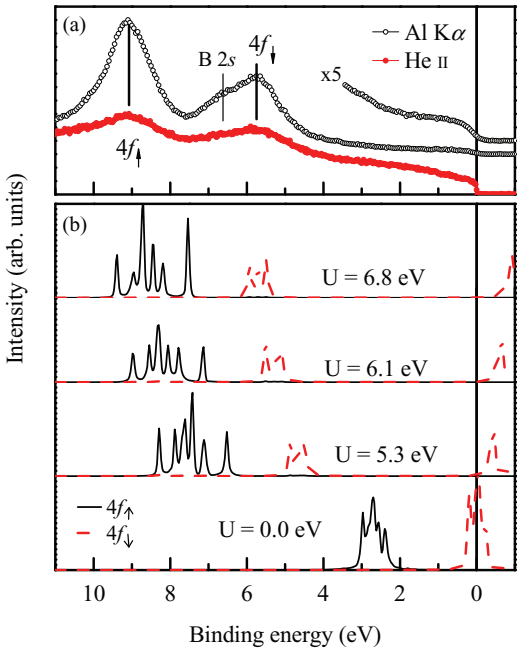

FIG. 4. (Color online) (a) Al $K\alpha$ and He II valence-band spectra. Near ϵ_F part of Al $K\alpha$ spectrum is shown in expanded scale. (b) Calculated partial density of states of Ho $4f$ up spin (solid line) and down spin (dashed line) are shown for different values of U.

B and C remain almost the same across all the temperatures studied. The peak position of the feature A exhibits different temperature dependence as shown in Fig. 3(f). The intensity of B relative to C increases in the 60° angled emission spectrum compared to the normal emission one suggesting dominant surface contribution in feature B.[18] The higher binding energy of the surface boron signal compared to the bulk signal can be associated to surface reconstruction, defects, surface inhomogeneity that may lead to an effective reduction of negative boron valency.

There are three inequivalent borons in the lattice as shown in Fig. 1. Since the number of neighbors and bond lengths are significantly different for octahedral borons (B1 and B3) and boron dimers (B2), the Madelung potential is expected to be different for these nonequivalent sites. Interestingly, the ratio of the integrated area of peaks A and C is about 1 : 2.8, which is similar to the number ratio of B2 and B1 + B3 (1 : 3). Thus, peak A can be attributed to B2 and C to the photoemission signals from B1 and B3. B2 dimers bridge the boron octahedra possessing large delocalized character compared to the octahedral borons leading to a larger width of feature A. The binding energy of the B 1*s* peak increases with the increase in temperature—the increase is much less for dimer borons relative to the octahedral ones. Such binding energy change indicates enhancement of negativity and/or ionicity of the corresponding borons with the decrease in temperature. Thus, $2p$ electrons of octahedral borons will gain significant local character at lower temperatures that could be related to the long-range order in the ground state.

The temperature evolution of the valence-band spectra is shown in Fig. 3(d). The spectral intensities in the vicinity of ϵ_F appears very similar within the energy resolution of Al $K\alpha$ spectroscopy. The features beyond 5-eV binding energy exhibit a small but gradual shift towards lower binding energies with the decrease in temperature (only two temperatures are shown for clarity in the figure). The energy shift is close to about 160 meV between 300 and 10 K.

Valence-band spectra collected using Al $K\alpha$ and He II photon energies are shown in Fig. 4. There are three distinct features around 5.8, 6.6, and 9.1 eV binding energies. The intensity of these features enhances significantly at Al $K\alpha$ photon energy. The comparison of the sensitivity of the peak intensities with the incident photon energy and the photoemission cross section[19] suggests large Ho $4f$ photoemission contribution in these peaks. The intensities near ϵ_F are primarily due to the B $2p$ contributions.

In order to clarify these assertions further, the energy-band structure of HoB_4 has been calculated within the local spin-density approximations in the full potential linearized augmented plane-wave method. Different effective on-site Coulomb correlation strength U_{eff} for the Ho $4f$ electrons has been considered to reproduce the experimental spectra. The calculated results are shown in Fig. 4(b). It is found that the electron correlation strength of about 7 eV produces the Ho $4f_\uparrow$ and $4f_\downarrow$ partial density of states at the peak positions observed in the experimental spectrum.

The partial densities of states (PDOS) corresponding to B $2p$ and Ho $5d$ states from the LDA calculations are shown in Fig. 5. B $2s$ states dominate between 5- and 10-eV binding energies. Thus, the features around 5.8 and 9.1 eV in the experimental spectrum can be attributed to Ho $4f_\downarrow$ and $4f_\uparrow$ contributions, respectively. The intensities around 6.6 eV are due to B $2s$ photoemission signal. Boron $2p$ states are dominated in the energy range −5 eV to ϵ_F. B1 and B3 $2p$

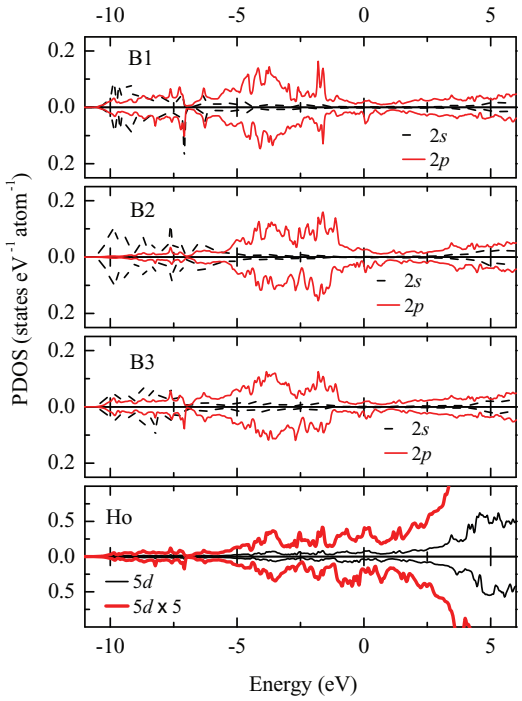

FIG. 5. (Color online) B 2s, B 2p, and Ho 5d partial density of states (PDOS) from the LSDA calculations. A rescaled Ho 5d PDOS (thick solid line in the bottom panel) is also shown for clarity.

PDOS have relatively larger contributions at higher binding energies possessing energy distributions similar to that of Ho 5d PDOS indicating stronger hybridization between the octahedral borons with Ho relative to the coupling of Ho with dimer borons, B2. Interestingly, the B1 contribution at higher binding energies is the largest suggesting strongest coupling with Ho moments.

The changes close to ϵ_F has been investigated with high-energy resolution using He I radiations. Since the electron escape depth at this energy is similar to the 60° angled emission in Al Kα spectra,[16] the identical spectral shape for normal emission and 60° angled emission shown in Fig. 2(c) established that the He I spectra would be representative of the bulk electronic structure. The raw data are shown in Fig. 6(a) exhibiting spectral evolution with significant spectral weight transfer across ϵ_F with temperature as expected in a system of fermions. Interestingly, the difference spectra $[I(T) - I(300\ \mathrm{K})]$ exhibit a larger change in spectral weight above ϵ_F relative to that below ϵ_F indicating a signature of particle-hole asymmetry.[20] Intensity at the Fermi level obtained by the symmetrization of the experimental spectra $[I(\epsilon - \epsilon_F) + I(\epsilon_F - \epsilon)]$ exhibits gradual decrease with the decrease in temperature. An additional sharp dip is observed in the 10-K data reflecting the signature of the long-range order in the ground state.[21] The spectral density of states (SDOS) obtained by the division with the Fermi-Dirac distribution function exhibit a similar line shape with $|\epsilon - \epsilon_F|^{0.5}$ dependence at all the temperatures.

Disorder due to the charge degrees of freedom has extensively been studied theoretically and experimentally.[22] Altshuler and Aronov showed that charge disorder induced effect in a correlated system exhibits $|\epsilon - \epsilon_F|^{0.5}$ dependence

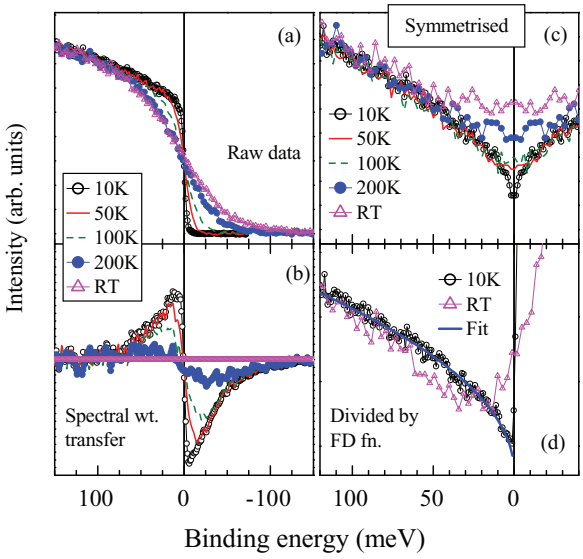

FIG. 6. (Color online) (a) High-resolution data close to the Fermi level at different temperatures. (b) Spectral weight transfer calculated by subtracting the 300-K data from all the raw data. (c) Symmetrized spectral density of states. (d) Spectral density of states obtained by the division with the resolution broadened Fermi function.

of the density of states near Fermi level.[23] Such disorder effect has been observed in a variety of systems such as $Ge_{1-x}Au_x$,[24] $Ni(S,Se)_2$,[25] oxides,[26] etc. Magnetic fluctuations often lead to a $|\epsilon - \epsilon_F|^{1.5}$ dependence of the spectral function[27] or $|\epsilon - \epsilon_F|^{0.25}$ in the vicinity of quantum critical behavior.[28] Evidently, the line shape of the density of states close to the Fermi level is sensitive to the electronic interaction parameters as well as disorder induced effects. In the present case, although the disorder is with respect to the spin-spin interactions, the spectral function exhibits a 0.5 exponent, similar to that predicted in Altshuler-Aronov theory. HoB_4 exhibits multiple long-range antiferromagnetic order with nonlinear magnetization direction. A change in the temperature and magnetic field influences the transport and magnetism in this system significantly suggesting an intimate relation between these two phenomena.[5] In addition, geometrical quadrupolar frustration has been observed in this compound indicating a strong spin-lattice interaction that might be the reason for the $|\epsilon - \epsilon_F|^{0.5}$ dependence of the spectral line shape. It would be interesting to see how the spectral function evolves in the proximity of the spin-liquid phase.

IV. CONCLUSION

In summary, the electronic structure of a noncollinear Shastry-Sutherland lattice system, HoB_4, is studied using high-resolution photoemission spectroscopy. The results show subtle differences and loss of boron at the surface compared to the bulk. Ho core-level spectra exhibit a signature of satellites suggesting the role of electron correlation among the conduction electrons. The valence-band spectra corresponding to the surface and bulk electronic structures are found to be similar. The spectral intensity near the Fermi level possess dominant 2p orbital character and exhibit disorder induced depletion of density of states. An additional sharp dip at 10 K

is observed that can be attributed to the long-range order in the ground state. Spectral weight transfer with temperature is found to be asymmetric with respect to ϵ_F revealing the signature of particle-hole asymmetry. The spectral line shape in the vicinity of the Fermi level in this spin-disordered system exhibits 0.5 exponent, which is similar to that found in the charge disordered system.

ACKNOWLEDGMENTS

The authors N.S. and K.M. acknowledge financial support from the Department of Science and Technology, Government of India under the Swarnajayanti fellowship program. G.B. acknowledges financial support from EPSRC, UK (EP/I007210/1).

*kbmaiti@tifr.res.in

[1] B. S. Shastry and B. Sutherland, Physica B & C **108**, 1069 (1981).

[2] J. Liu, N. Trivedi, Y. Lee, B. N. Harmon, and J. Schmalian, Phys. Rev. Lett. **99**, 227003 (2007).

[3] S. Miyahara and K. Ueda, J. Phys.: Condens. Matter **15**, R327 (2003).

[4] S. Ji, C. Song, J. Koo, K.-B. Lee, Y. J. Park, J. Y. Kim, J.-H. Park, H. J. Shin, J. S. Rhyee, B. H. Oh, and B. K. Cho, Phys. Rev. Lett. **91**, 257205 (2003); R. Watanuki, H. Mitamura, T. Sakakibara, G. Sato, and K. Suzuki, Physica B **378–380**, 594 (2006); F. Iga, A. Shigekawa, Y. Hasegawa, S. Michimura, T. Takabatake, S. Yoshii, T. Yamamoto, M. Hagiwara, and K. Kindo, J. Magn. Magn. Mater. **310**, e443 (2007).

[5] S. Ji, C. Song, J. Koo, J. Park, Y. J. Park, K.-B. Lee, S. Lee, J.-G. Park, J. Y. Kim, B. K. Cho, K.-P. Hong, C.-H. Lee, and F. Iga, Phys. Rev. Lett. **99**, 076401 (2007).

[6] K. H. J. Buschow and J. H. N. Creyghton, J. Chem. Phys. **57**, 3910 (1972).

[7] H. C. Choi, A. Laref, J. H. Shim, S. K. Kwon, and B. I. Min, J. Appl. Phys. **105**, 07E107 (2009).

[8] Z. P. Yin and W. E. Pickett, Phys. Rev. B **77**, 035135 (2008).

[9] T. Matsumura, D. Okuyama, and Y. Murakami, J. Phys. Soc. Jpn. **76**, 015001 (2007).

[10] Z. Fisk, M. B. Maple, D. C. Jonhnston, and L. D. Woolf, Solid State Commun. **39**, 1189 (1981).

[11] D. Okuyama, T. Matsumura, K. Iwasa, and Y. Murakami, J. Magn. Magn. Mater. **310**, e152 (2007).

[12] J. Y. Kim, B. K. Cho, and S. H. Han, J. Appl. Phys. **105**, 07E116 (2009).

[13] G. Balakrishnan, M. R. Lees, and D. Paul, J. Cryst. Growth **256**, 206 (2003); J. Magn. Magn. Mater. **272–276**, 601 (2004).

[14] P. Blaha, K. Schwarz, G. K. H. Madsen, D. Kvasnicka, and J. Luitz, *WIEN2k, An Augmented Plane Wave + Local Orbitals Program for Calculating Crystal Properties* (Karlheinz Schwarz, Techn. Universität Wien, Austria, 2001).

[15] V. I. Anisimov, I. V. Solovyev, M. A. Korotin, M. T. Czyzyk, and G. A. Sawatzky, Phys. Rev. B **48**, 16929 (1993).

[16] K. Maiti, U. Manju, S. Ray, P. Mahadevan, I. H. Inoue, C. Carbone, and D. D. Sarma, Phys. Rev. B **73**, 052508 (2006); K. Maiti, A. Kumar, D. D. Sarma, E. Weschke, and G. Kaindl, *ibid.* **70**, 195112 (2004); R. S. Singh and K. Maiti, *ibid.* **76**, 085102 (2007).

[17] K. Maiti and R. S. Singh, Phys. Rev. B **71**, 161102(R) (2005); K. Maiti, Solid State Commun. **149**, 1351 (2009).

[18] S. Patil, G. Adhikary, G. Balakrishnan, and K. Maiti, Solid State Commun. **151**, 326 (2011).

[19] S. Hüfner, *Photoelectron Spectroscopy* (Springer, Berlin, 1995); J. J. Yeh and I. Lindau, At. Data Nucl. Data Tables **32**, 1 (1985); K. Maiti and D. D. Sarma, Phys. Rev. B **58**, 9746 (1998).

[20] K. Maiti, R. S. Singh, and V. R. R. Medicherla, Europhys. Lett. **78**, 17002 (2007).

[21] R. S. Singh, V. R. R. Medicherla, and K. Maiti, Appl. Phys. Lett. **91**, 132503 (2007); G. Adhikary, R. Bindu, S. Patil, and K. Maiti, *ibid.* **100**, 042401 (2012).

[22] P. A. Lee and T. V. Ramakrishnan, Rev. Mod. Phys. **57**, 287 (1985).

[23] B. L. Altshuler and A. G. Aronov, Solid State Commun. **30**, 115 (1979).

[24] W. L. McMillan and J. Mochel, Phys. Rev. Lett. **46**, 556 (1981).

[25] D. D. Sarma, A. Chainani, S. R. Krishnakumar, E. Vescovo, C. Carbone, W. Eberhardt, O. Rader, Ch. Jung, Ch. Hellwig, W. Gudat, H. Srikanth, and A. K. Raychaudhuri, Phys. Rev. Lett. **80**, 4004 (1998).

[26] M. Kobayashi, K. Tanaka, A. Fujimori, S. Ray, and D. D. Sarma, Phys. Rev. Lett. **98**, 246401 (2007).

[27] K. Maiti, R. S. Singh, V. R. R. Medicherla, S. Rayaprol, and E. V. Sampathkumaran, Phys. Rev. Lett. **95**, 016404 (2005); K. Maiti, R. S. Singh, and V. R. R. Medicherla, Phys. Rev. B **76**, 165128 (2007); R. S. Singh, V. R. R. Medicherla, Kalobaran Maiti, and E. V. Sampathkumaran, *ibid.* **77**, 201102(R) (2008).

[28] G. Adhikary, R. Bindu, S. K. Pandey, and K. Maiti, Europhys. Lett. **99**, 37009 (2012).